

Supporting Information (SI)

Zwitterionic fused pyrazolo-triazole based high performing energetic materials

Parasar Kumar,^{a,‡} Navaneet Kumar,^{a,‡} Vikas D. Ghule,^b Srinivas Dharavath^{a*}

^aEnergetic Materials Laboratory, Department of Chemistry, Indian Institute of Technology Kanpur, Kanpur-208016, Uttar Pradesh, India.

E-mail: srinivasd@iitk.ac.in, <https://www.energeticslab.com/>

^bDepartment of Chemistry, National Institute of Technology Kurukshetra, Kurukshetra-136119, Haryana, India.

[‡] Contributed equally

Table of Contents

General methods	S2
Experimental section	S2-S4
Crystal structure for 2 .	S4-S8
NMR, IR, HRMS spectrum & TGA-DSC plots for 2 to 5 .	S9-S20
Computational details	S21-S28
References	S28

Caution! All the compounds investigated are potentially explosive, energetic materials. Although we have experienced no difficulties in syntheses and characterization of these compounds, manipulations must be carried out by using appropriate standard safety precautions. Eye protection and leather gloves must be always worn.

General Methods

Reagents were purchased from Ak Scientifics, Acros Organics or Aldrich as analytical grade and were used as received. ¹H NMR, ¹³C NMR spectra were recorded using JEOL DELTA (ECS) 500 (¹H, 500 MHz; ¹³C, 126 MHz) nuclear magnetic resonance spectrometer. DMSO-d₆ was employed as the solvent and locking solvent. Chemical shifts are given relative to (CH₃)₄Si for ¹H and ¹³C spectra. Decomposition temperatures (onset) were recorded using a dry nitrogen gas purge and at heating rate of 5 °C min⁻¹ on a differential scanning calorimeter (SDT650) using compound in the range of 1.5- 2 mg. IR spectra were recorded using Zn-Se pellets with ECO-ATR spectrometer (Bruker Alpha II). Density was determined at room temperature by employing Anton Par Ultra5000 gas pycnometer in helium atmosphere. Impact and friction-sensitivity measurements were tested by employing a standard BAM Fall hammer and a BAM friction tester. The single-crystal X-ray data collection was carried out using Bruker APEX-II CCD diffractometer. The crystal was kept at 100 K during data collection.

Experimental Section:

Synthesis of 3,5-dihydrazineyl-4-nitro-1H-pyrazole (1): 4,6-dichloro-5-nitropyrimidine (2 g, 10.31 mmol) was taken in hydrazine monohydrate and heated at 120 °C for 4 hrs. The reaction mixture was cooled to room temperature and kept in refrigerator for overnight. The newly formed yellow precipitate was collected by filtration, washed with cold water, ethanol (30 mL) and dried in oven overnight at 60 °C to get compound **1** in 30% yield (536 mg, 3.09 mmol). ¹H NMR (500 MHz, DMSO-d₆): δ (ppm) 4.33 (s, 4H), 6.05 (s, 1H), 7.6 (s, 2H). ¹³C NMR (126 MHz, DMSO-d₆): δ(ppm) 106.12, 151.23. IR (ATR, ZnSe, cm⁻¹): 723, 990, 1138, 1168, 1323, 1403, 1523, 1635, 3220, 3299. Elemental analysis: (%) calculated for C₃H₇N₇O₂(0.1 EtOH): C, 21.62; H, 4.31; N, 55.16. Found: C, 21.59; H, 4.43; N, 55.32.

Synthesis of 3-amino-6-hydrazineyl-7-nitropyrazolo[5,1-c][1,2,4]triazol-2-ium-5-ide (2) : Compound **1** (300 mg, 1.73 mmol) was taken in dil. HCl (1M, 20 ml) and stirred at room temperature for 2 to 3 minutes. To this, cyanogen bromide (276 mg, 2.5 mmol) was added,

and reaction mixture was stirred at same temperature. It slowly started precipitating after one hour and same was continued for another 30 hours and monitored by thin layer chromatography (TLC). The newly formed light-yellow precipitate was collected by filtration and washed with cold water, dried in oven overnight at 60 °C to obtain pure compound **2** in 86 % yield (296 mg, 1.5 mmol). $T_d(\text{onset})$: 250 °C. $^1\text{H NMR}$ (500 MHz, DMSO-d_6): δ (ppm) 7.07 (br, 4H), 9.19 (s, 2H). $^{13}\text{C NMR}$ (126 MHz, DMSO-d_6): δ (ppm) 102.9, 141.4, 143.3, 154.7. IR (ATR, ZnSe, cm^{-1}): 552, 744, 1079, 1143, 1197, 1345, 1439, 1500, 1646, 1689, 2652, 3106, 3294. Elemental analysis: (%) calculated for $\text{C}_4\text{H}_6\text{N}_8\text{O}_2 \cdot 1.3\text{HCl}$ (198.14): C, 19.57; H, 3.00; N, 45.64; found C, 19.68; H, 3.42; N, 45.17.



General procedure for the synthesis of salts 3-5: Compound **2** (300 mg, 1.51 mmol) was taken in methanol (15 ml) and hydroxyl amine hydrate (95 μl , 2.2 mmol), hydrazine monohydrate (111 μl , 2.2 mmol), and 3,6,7-triamino-7*H*-[1,2,4]triazolo[4,3-*b*][1,2,4]triazol-2-ium (TATOT) (279 mg, 1.81 mmol) was added in to it and stirred at room temperature for 12 hours. The formed precipitate was collected by filtration and washed with methanol and dried in oven overnight at 60 to 70 °C to get pure products in quantitative yields.

Synthesis of hydroxylammonium-3-amino-6-hydrazineyl-7-nitropyrazolo[5,1-*c*][1,2,4]triazol-5-ide (3) : Dark Yellow. Yield 88 % (308 mg, 1.33 mmol). $T_d(\text{onset})$: 262 °C. $^1\text{H NMR}$ (500 MHz, DMSO-d_6): δ (ppm) 6.84 (s, 6H), 7.67 (s, 3H). $^{13}\text{C NMR}$ (126 MHz, DMSO-d_6): δ (ppm) 102.3, 141.3, 143.4, 159.2. IR (ATR, ZnSe, cm^{-1}): 589, 805, 1114, 1173, 1309, 1517, 1561, 1696, 2796, 3193, 3296, 3381. Elemental analysis: (%) calculated for $\text{C}_4\text{H}_9\text{N}_9\text{O}_3$ (231.17): C, 23.78; H, 3.22; N, 55.53; found C, 24.03; H, 3.15; N, 55.67.



Synthesis of hydrazinium-3-amino-6-hydrazineyl-7-nitropyrazolo[5,1-c][1,2,4]triazol-5-ide (4) : Dark yellow. Yield 93 % (325 mg, 1.41 mmol). $T_d(\text{onset})$: 171 °C. $^1\text{H NMR}$ (500 MHz, DMSO-d_6): δ (ppm) 6.22 (br, 8H), 7.58 (s, 2H). $^{13}\text{C NMR}$ (126 MHz, DMSO-d_6): δ (ppm) 102.5, 143, 143.6, 159.5. IR (ATR, ZnSe, cm^{-1}): 522, 804, 1109, 1173, 1309, 1508, 1559, 1626, 1694, 2955, 3187, 3296. Elemental analysis: (%) calculated for $\text{C}_4\text{H}_{10}\text{N}_{10}\text{O}_2 \cdot 0.1 \text{ MeOH}$ (230.19): C, 21.10; H, 4.49; N, 60.01; found C, 21.89; H, 3.87.; N, 59.10.



Synthesis of 3,6,7-triamino-7H-[1,2,4]triazolo[4,3-b][1,2,4]triazol-2-ium-3-amino-6-hydrazineyl-7-nitropyrazolo[5,1-c][1,2,4]triazol-5-ide (5): Dark yellow. Yield 82% (437 g, 1.24 mmol). $T_d(\text{onset})$: 240 °C. $^1\text{H NMR}$ (500 MHz, DMSO-d_6): δ (ppm) 5.72 (s, 2H), 6.8 (s, 4H), 6.99 (s, 2H), 7.72 (s, 1H). $^{13}\text{C NMR}$ (126 MHz, DMSO-d_6): δ (ppm) 102.3, 141.5, 142.6, 143.3, 143.9, 148.4, 159.3. IR (ATR, ZnSe, cm^{-1}): 524, 551, 666, 788, 1044, 1134, 1310, 1350, 1433, 1520, 1593, 1651, 3007, 3297, 3396. Elemental analysis: (%) calculated for $\text{C}_7\text{H}_{12}\text{N}_{16}\text{O}_2$ (352.28): C, 23.87; H, 3.43; N, 63.62; found C, 23.54; H, 3.48; N, 64.36.

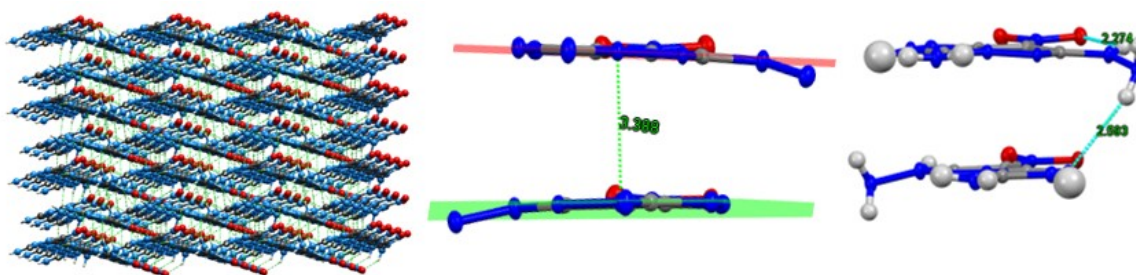


Figure S1: Crystal packing (with weak interactions), interplanar distances and intramolecular and intermolecular H-bonding interaction of **2**.

Table S1: Crystallographic data for 2.

CCDC	2288301
Empirical formula	C ₄ H ₆ N ₈ O ₂
Formula weight	198.17
Temperature/K	100
Crystal system	orthorhombic
Space group	<i>Pna2</i> ₁
<i>a</i> /Å	6.744(2)
<i>b</i> /Å	11.212(2)
<i>c</i> /Å	9.487(2)
α /°	90.00(3)
β /°	90.00(3)
γ /°	90.00(3)
Volume/Å ³	717.3(3)
<i>Z</i>	4
ρ calc/cm ³	1.835
μ /mm ⁻¹	0.151
<i>F</i> (000)	408.0
Crystal size/mm ³	0.2 × 0.15 × 0.1
Radiation	MoK α (λ = 0.71073)
2 Θ range for data collection/°	5.626 to 56.568
Index ranges	-8 ≤ <i>h</i> ≤ 8, -14 ≤ <i>k</i> ≤ 14, -12 ≤ <i>l</i> ≤ 12
Reflections collected	11348
Independent reflections	1788 [Rint = 0.0690, Rsigma = 0.0412]
Data/restraints/parameters	1788/1/136
Goodness-of-fit on <i>F</i> ²	1.042
Final <i>R</i> indexes [<i>I</i> ≥ 2 σ (<i>I</i>)]	<i>R</i> 1 = 0.0375, <i>wR</i> 2 = 0.0893
Final <i>R</i> indexes [all data]	<i>R</i> 1 = 0.0458, <i>wR</i> 2 = 0.0948
Largest diff. peak/hole / e Å ⁻³	0.30/-0.27
Flack parameter	-0.7(10)

Table 2: Fractional Atomic Coordinates (×10⁴) and Equivalent Isotropic Displacement Parameters (Å²×10³) for **2**. *U*_{eq} is defined as 1/3 of the trace of the orthogonalised *U*_{ij} tensor.

Atom	<i>x</i>	<i>y</i>	<i>z</i>	<i>U</i> (eq)
O001	2546(4)	6725.0(18)	8324(3)	21.0(5)
O002	2772(3)	8659.1(18)	7935(2)	21.2(5)
N003	2991(4)	7581(2)	7539(3)	16.4(5)
N004	4554(4)	7646(2)	4018(3)	15.7(5)
N005	4688(4)	9498(2)	3556(3)	17.2(5)
N006	4589(4)	6395(2)	4171(3)	15.4(5)
N007	4158(4)	9444(2)	4982(3)	17.6(5)
N008	3919(4)	5191(2)	6134(3)	17.3(5)

N009	4682(4)	4172(2)	5457(3)	19.8(6)
N00A	5543(4)	8174(2)	1670(3)	21.9(6)
C1	4977(4)	8423(3)	2964(3)	16.8(6)
C4	4053(4)	6270(3)	5511(3)	15.8(6)
C2	4079(4)	8288(3)	5199(3)	15.3(6)
C3	3672(4)	7395(2)	6223(3)	15.7(6)

Table 3: Anisotropic Displacement Parameters ($\text{\AA}^2 \times 10^3$) for **2**. The Anisotropic displacement factor exponent takes the form: $-2\pi^2[h^2a^2U_{11}+2hka*b*U_{12}+\dots]$.

Atom	U11	U22	U33	U23	U13	U12
O001	27.2(11)	17.6(11)	18.2(10)	3.0(9)	2.2(8)	-2.9(9)
O002	23.9(11)	14.3(10)	25.4(11)	-5.6(9)	3.5(10)	-2.3(8)
N003	15.3(11)	14.2(11)	19.8(13)	-1.0(9)	-0.3(10)	-1.8(9)
N004	19.7(13)	9.7(11)	17.7(12)	0.9(10)	-0.7(10)	-0.6(10)
N005	22.8(13)	10.9(11)	17.9(13)	1.8(10)	1.3(11)	-0.3(10)
N006	18.1(12)	7.1(10)	20.9(12)	2.5(10)	-1.8(10)	-0.8(10)
N007	18.9(12)	14.2(12)	19.6(13)	-0.4(10)	-0.3(11)	-1.0(9)
N008	23.8(13)	9.6(11)	18.7(12)	1.2(10)	2.6(11)	1.6(9)
N009	25.5(14)	12.9(12)	20.9(14)	-1.8(10)	-0.6(11)	3.1(10)
N00A	34.4(16)	12.6(11)	18.8(13)	2.8(11)	3.4(12)	-0.3(10)
C1	17.2(13)	13.1(13)	20.2(15)	2.8(12)	-1.4(12)	-1.0(10)
C4	14.7(14)	13.7(14)	18.9(15)	0.5(11)	-3.2(12)	-1.7(11)
C2	14.8(13)	12.4(13)	18.8(15)	-0.1(12)	-1.5(11)	0.4(10)
C3	16.5(13)	13.2(12)	17.5(14)	2.7(12)	-2.0(12)	-1.5(10)

Table S4: Bond Lengths for **2**.

Atom	Atom	Length/ \AA	Atom	Atom	Length/ \AA
------	------	----------------------	------	------	----------------------

O001	N003	1.251(3)	N006	C4	1.329(4)
O002	N003	1.275(3)	N007	C2	1.313(4)
N003	C3	1.347(4)	N008	N009	1.408(3)
N004	N006	1.410(3)	N008	C4	1.349(4)
N004	C1	1.356(4)	N00A	C1	1.316(4)
N004	C2	1.369(4)	C4	C3	1.453(4)
N005	N007	1.401(4)	C2	C3	1.421(4)
N005		C1		1.344(4)	

Table S5: Bond Angles for **2**.

Atom	Atom	Atom	Angle/°	Atom	Atom	Atom	Angle/°
O001	N003	O002	121.6(3)	N00A	C1	N004	127.8(3)
O001	N003	C3	121.0(2)	N00A	C1	N005	128.4(3)
O002	N003	C3	117.4(2)	N006	C4	N008	122.1(3)
C1	N004	N006	135.3(3)	N006	C4	C3	113.6(2)
C1	N004	C2	108.3(2)	N008	C4	C3	124.2(3)
C2	N004	N006	116.2(2)	N004	C2	C3	103.5(2)
C1	N005	N007	113.6(3)	N007	C2	N004	112.4(3)
C4	N006	N004	101.5(2)	N007	C2	C3	144.1(3)
C2	N007	N005	101.8(2)	N003	C3	C4	128.7(2)
C4	N008	N009	120.2(3)	N003	C3	C2	126.1(3)
N005	C1	N004	103.8(3)	C2	C3	C4	105.1(2)

Table S6: Torsion Angles for **2**.

A	B	C	D	Angle/°	A	B	C	D	Angle/°
O001	N003	C3	C4	-1.7(4)	N007	N005	C1	N004	2.2(3)
O001	N003	C3	C2	174.8(3)	N007	N005	C1	N00A	-177.6(3)
O002	N003	C3	C4	-180.0(3)	N007	C2	C3	N003	5.0(6)
O002	N003	C3	C2	-3.5(4)	N007	C2	C3	C4	-177.8(4)
N004	N006	C4	N008	-178.8(3)	N008	C4	C3	N003	-5.7(5)
N004	N006	C4	C3	0.1(3)	N008	C4	C3	C2	177.2(3)
N004	C2	C3	N003	-174.7(3)	N009	N008	C4	N006	11.4(4)
N004	C2	C3	C4	2.5(3)	N009	N008	C4	C3	-167.5(3)
N005	N007	C2	N004	1.0(3)	C1	N004	N006	C4	177.9(3)
N005	N007	C2	C3	-178.8(4)	C1	N004	C2	N007	0.3(4)
N006	N004	C1	N005	-177.8(3)	C1	N004	C2	C3	-179.9(2)
N006	N004	C1	N00A	1.9(6)	C1	N005	N007	C2	-2.0(3)
N006	N004	C2	N007	177.4(3)	C2	N004	N006	C4	1.7(3)
N006	N004	C2	C3	-2.7(3)	C2	N004	C1	N005	-1.4(3)
N006	C4	C3	N003	175.4(3)	C2	N004	C1	N00A	178.3(3)
N006		C4		C3		C2			-1.7(3)

Table S7: Hydrogen Atom Coordinates ($\text{\AA}\times 10^4$) and Isotropic Displacement Parameters ($\text{\AA}^2\times 10^3$) for **2**.

Atom	<i>x</i>	<i>y</i>	<i>z</i>	U(eq)
H008	3353.36	5124.05	6966.47	21
H00A	3928.88	3990.42	4756.21	24
H00C	5783.44	8755.35	1070.4	26
H00D	5680.19	7426.99	1404.26	26

H00B	5940(50)	4310(40)	5170(40)	25(10)
H005	5110(80)	10130(60)	3130(70)	84(19)

NMR, IR Spectra, HRMS & TG-DSC plots for 1-5.

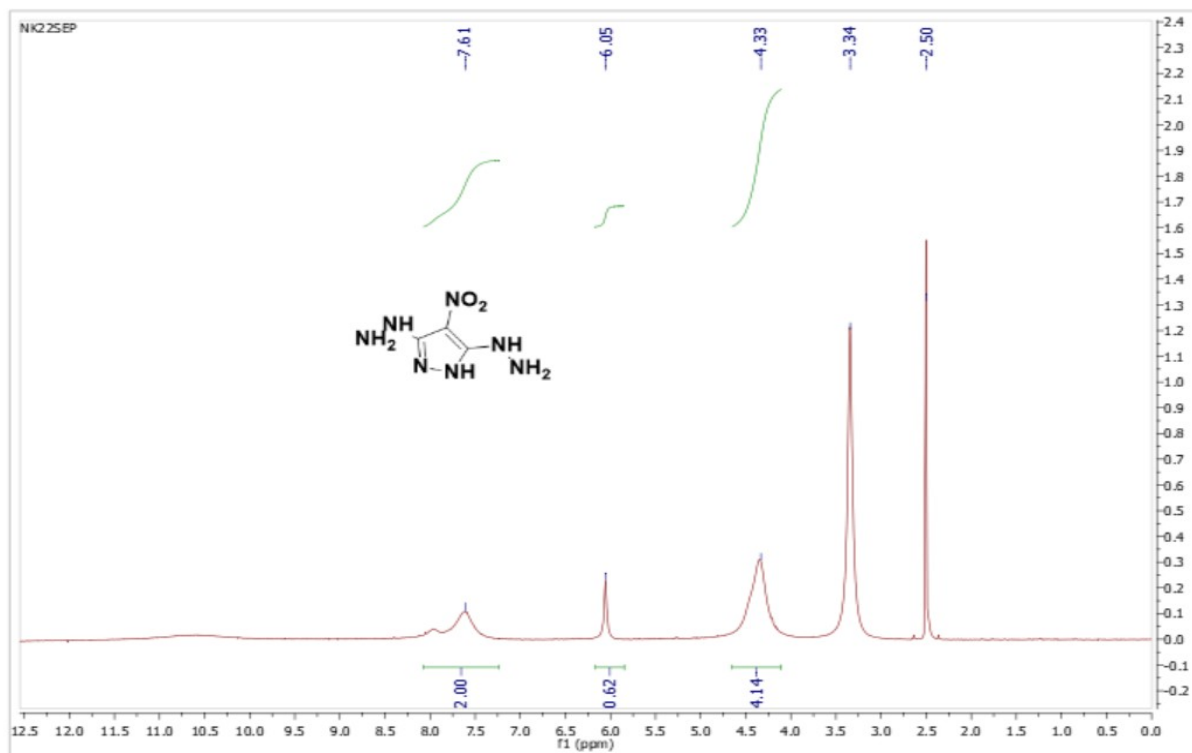


Figure S2: ¹H NMR spectrum of compound 1 in DMSO-d₆.

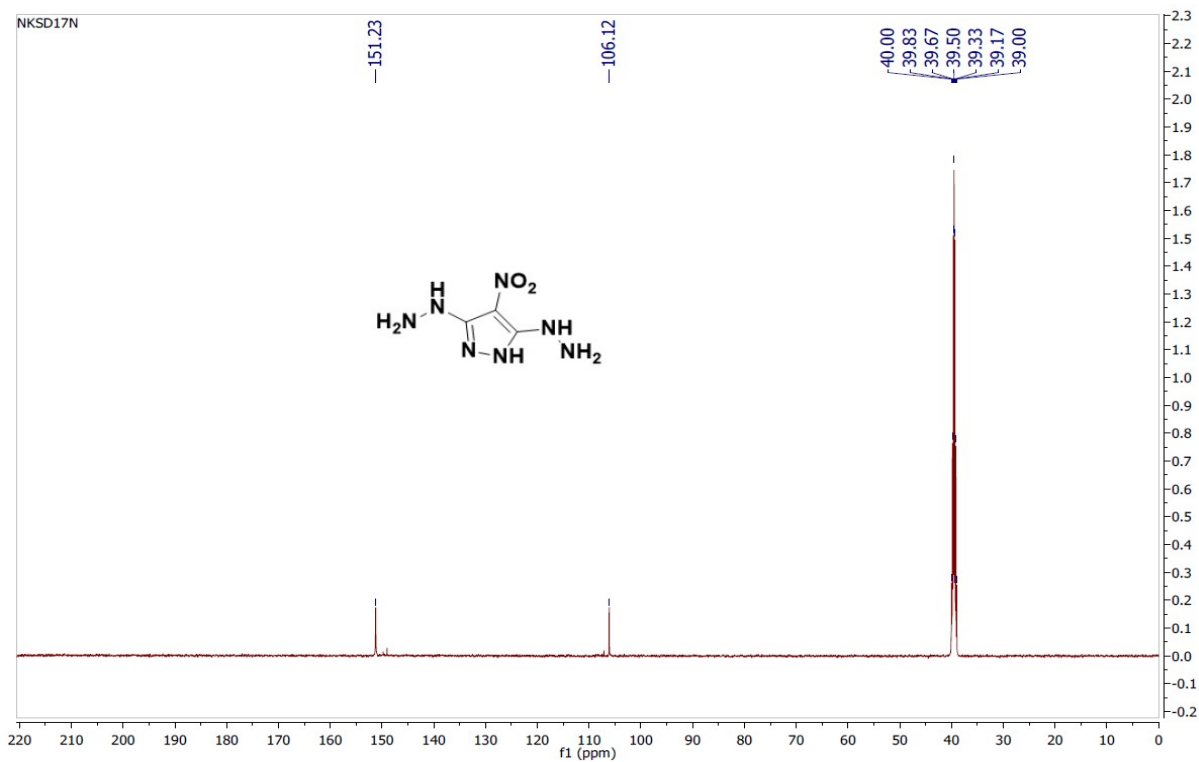


Figure S3: ¹³C NMR spectrum of compound 1 in DMSO-*d*₆.

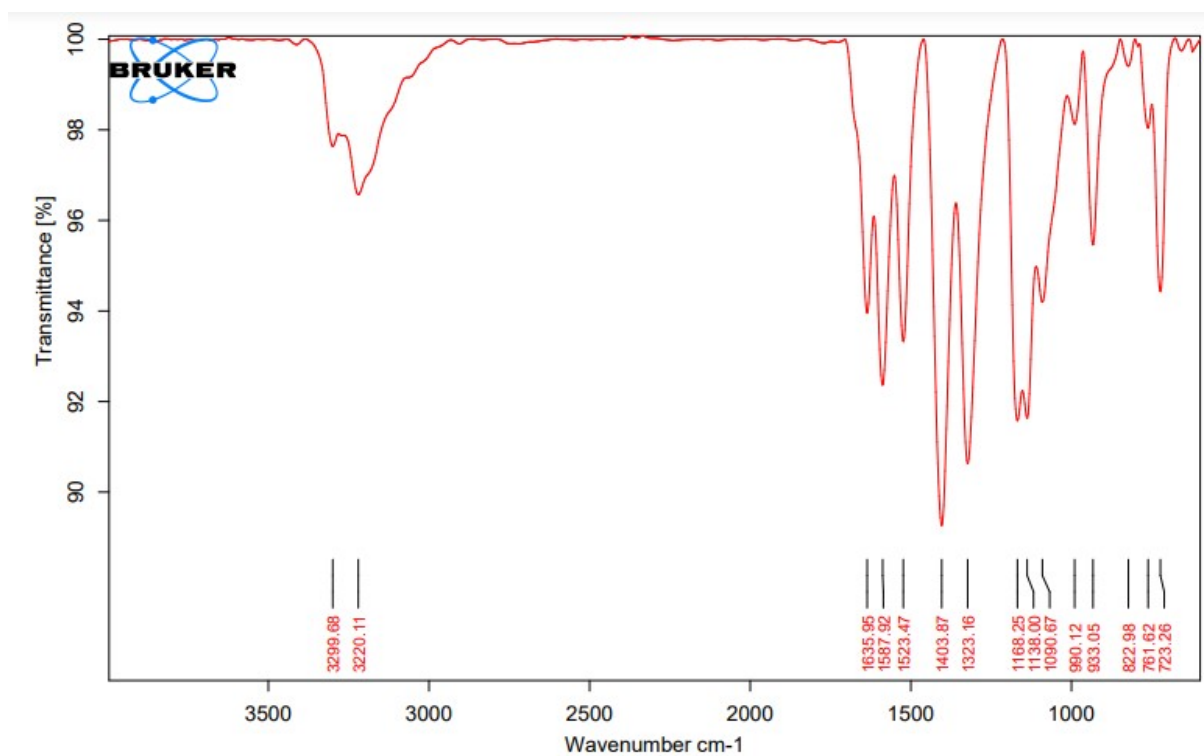


Figure S4: IR spectrum of compound 1.

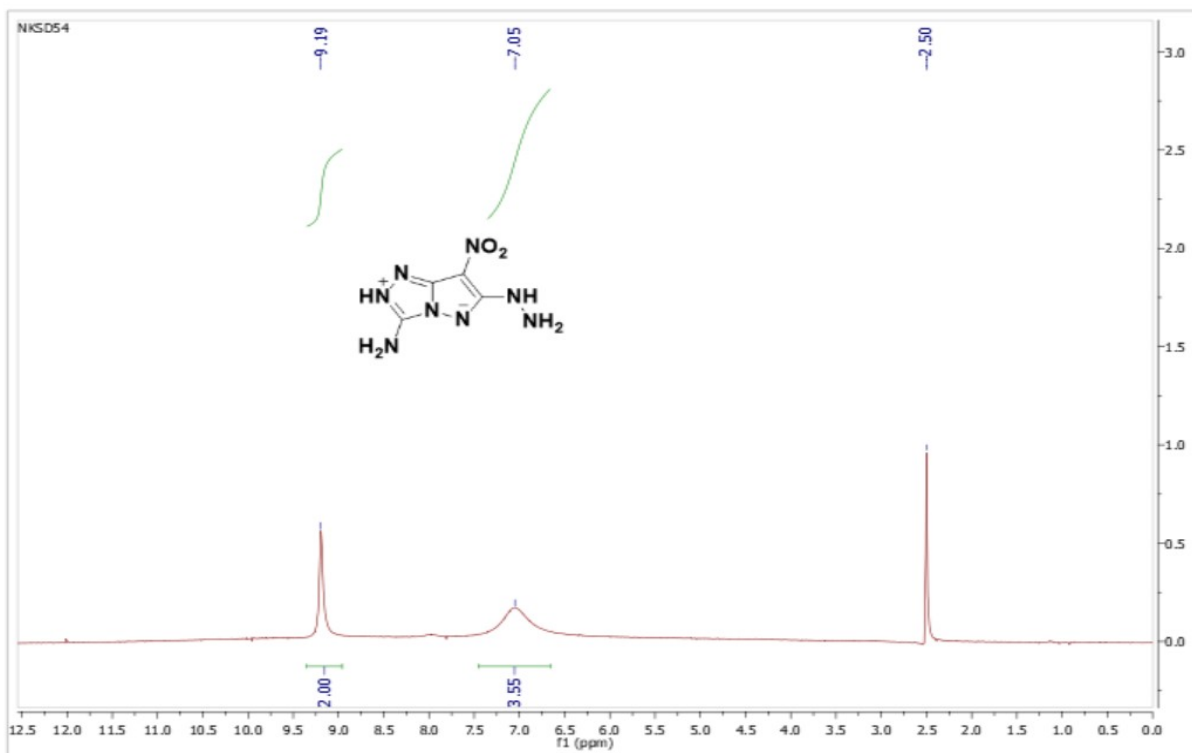


Figure S5: ^1H NMR spectrum of compound **2** in $\text{DMSO-}d_6$.

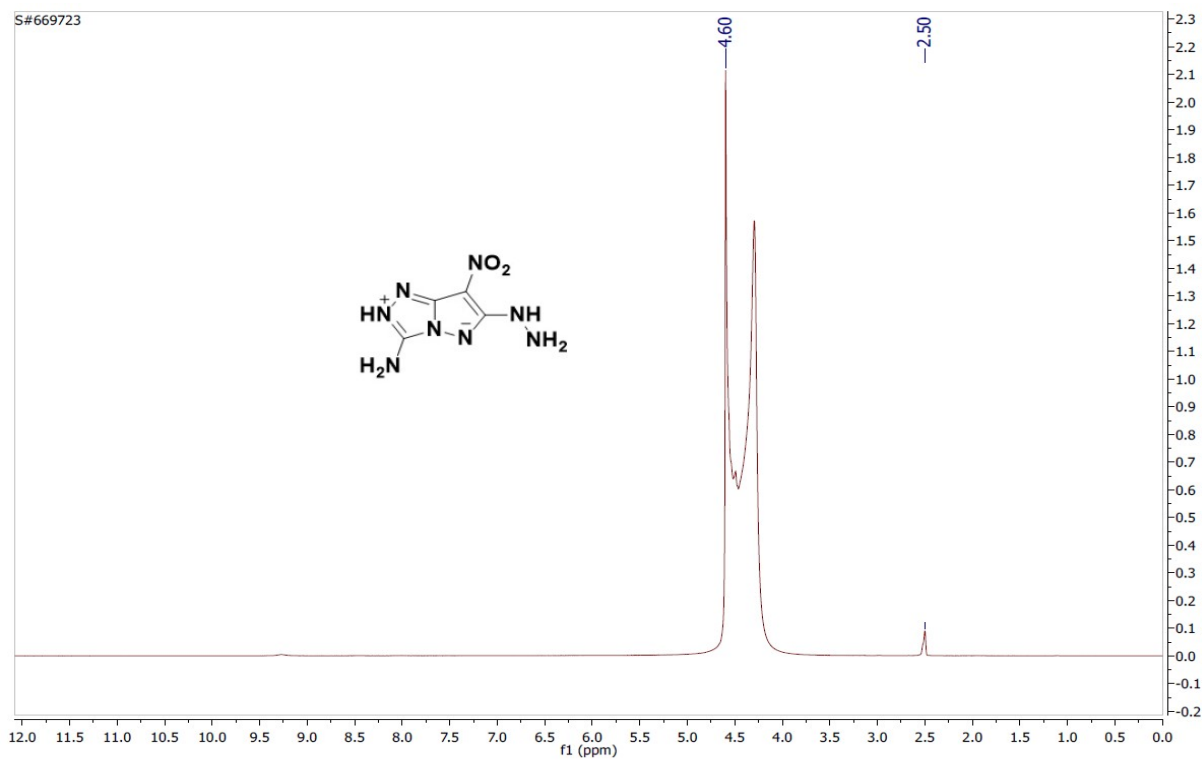


Figure S6: ^1H NMR spectrum of compound **2** in D_2O .

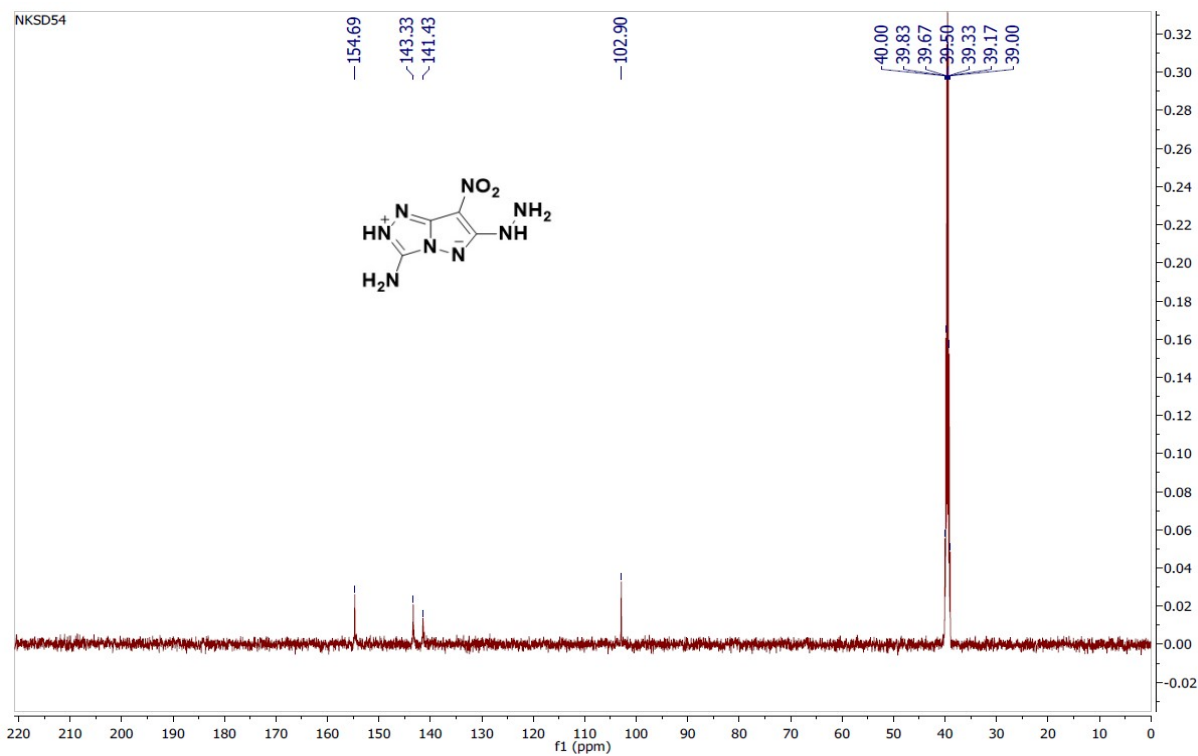


Figure S7: ¹³C NMR spectrum of compound 2 in DMSO-*d*₆.

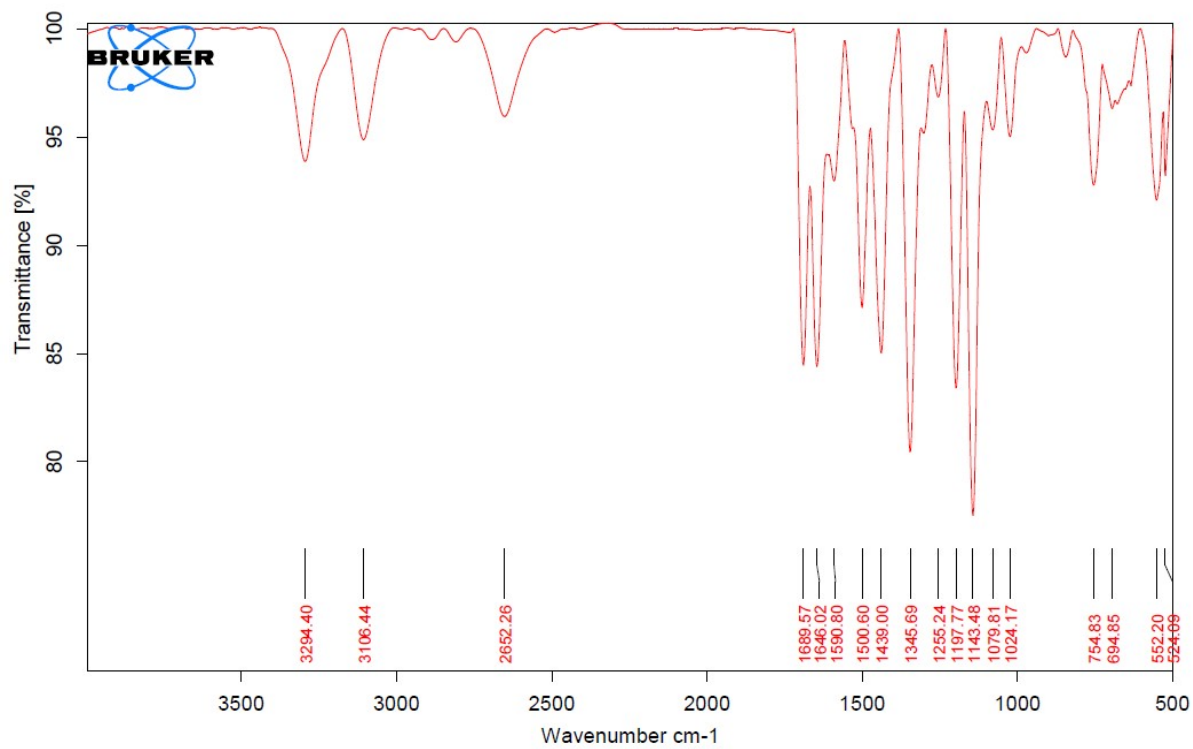
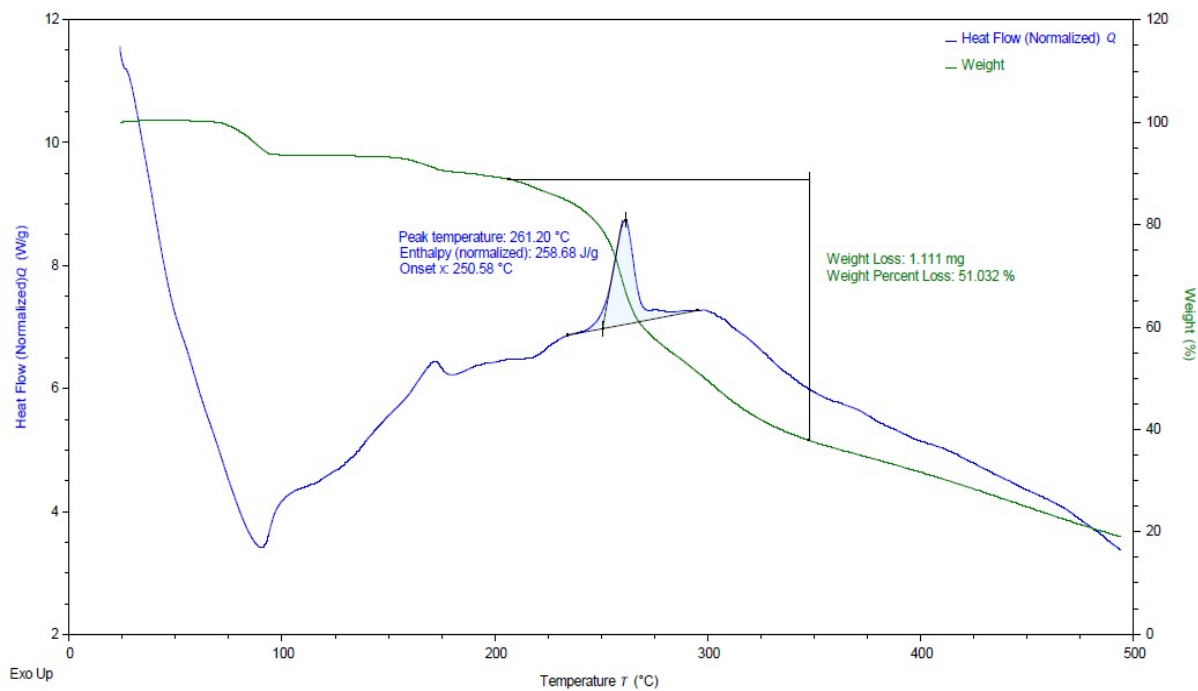


Figure S8: IR spectrum of compound 2.



TA Instruments Trios V5.5.0.323

Figure S9: DSC spectra of compound **2** at heating rate 5 °C min⁻¹.

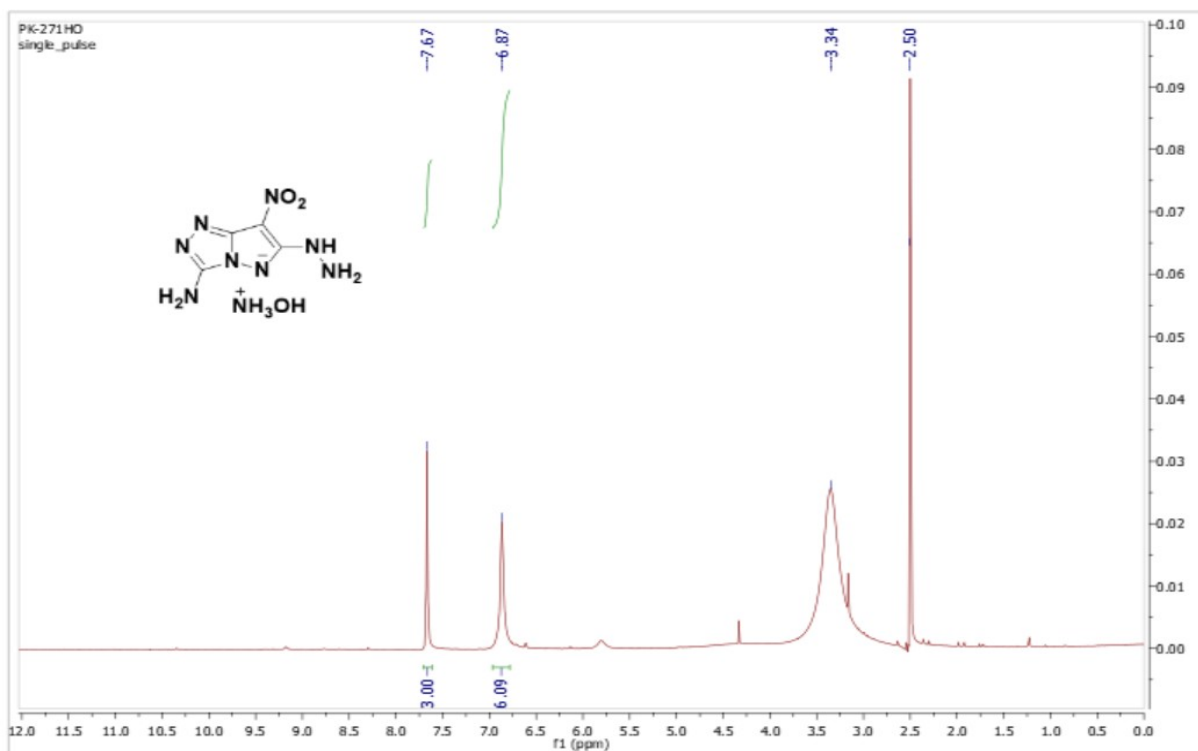


Figure S10: ¹H NMR spectrum of compound **3** in DMSO-*d*₆.

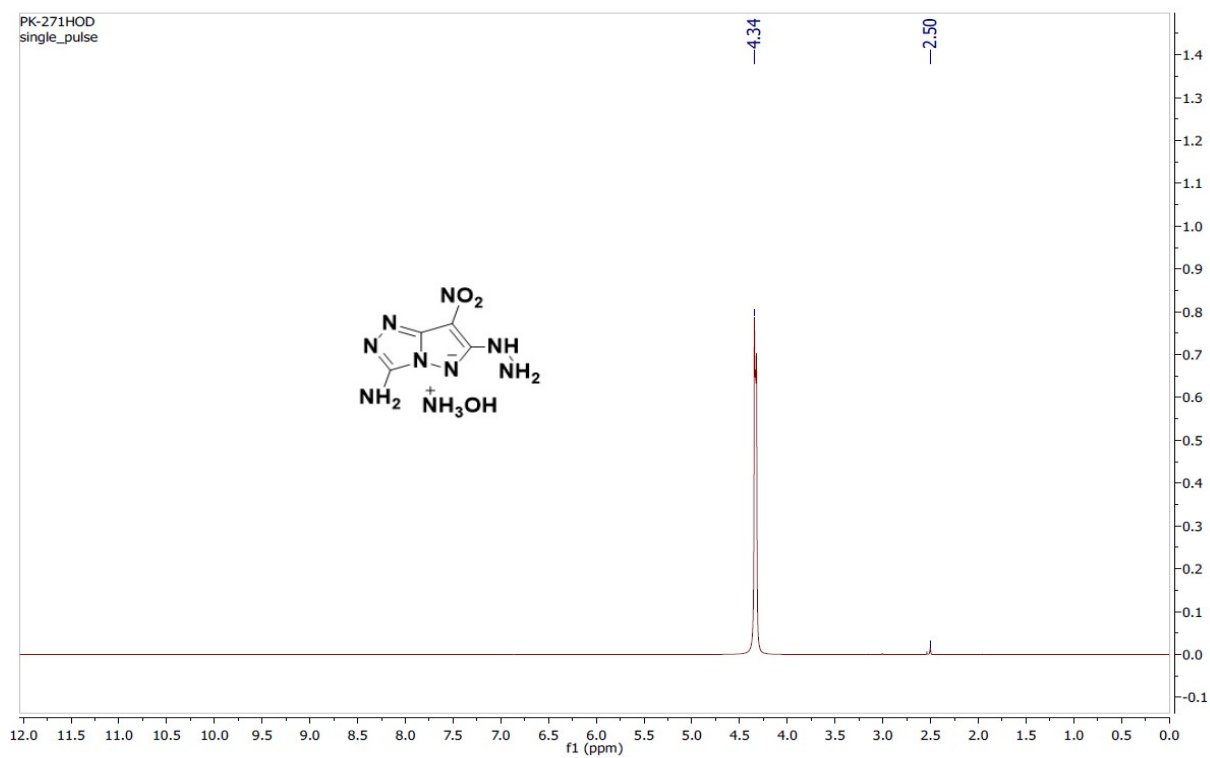


Figure S11: ^1H NMR spectrum of compound 3 in D_2O .

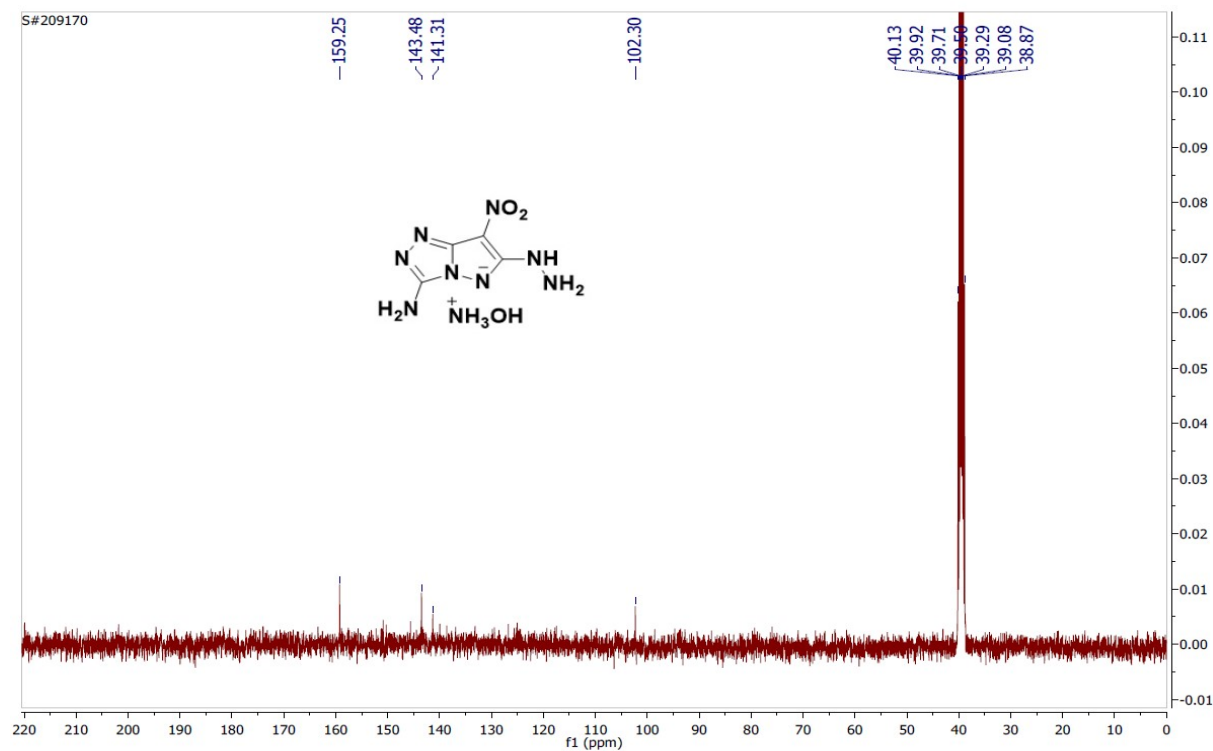


Figure S12: ^{13}C NMR spectrum of compound 3 in $\text{DMSO-}d_6$.

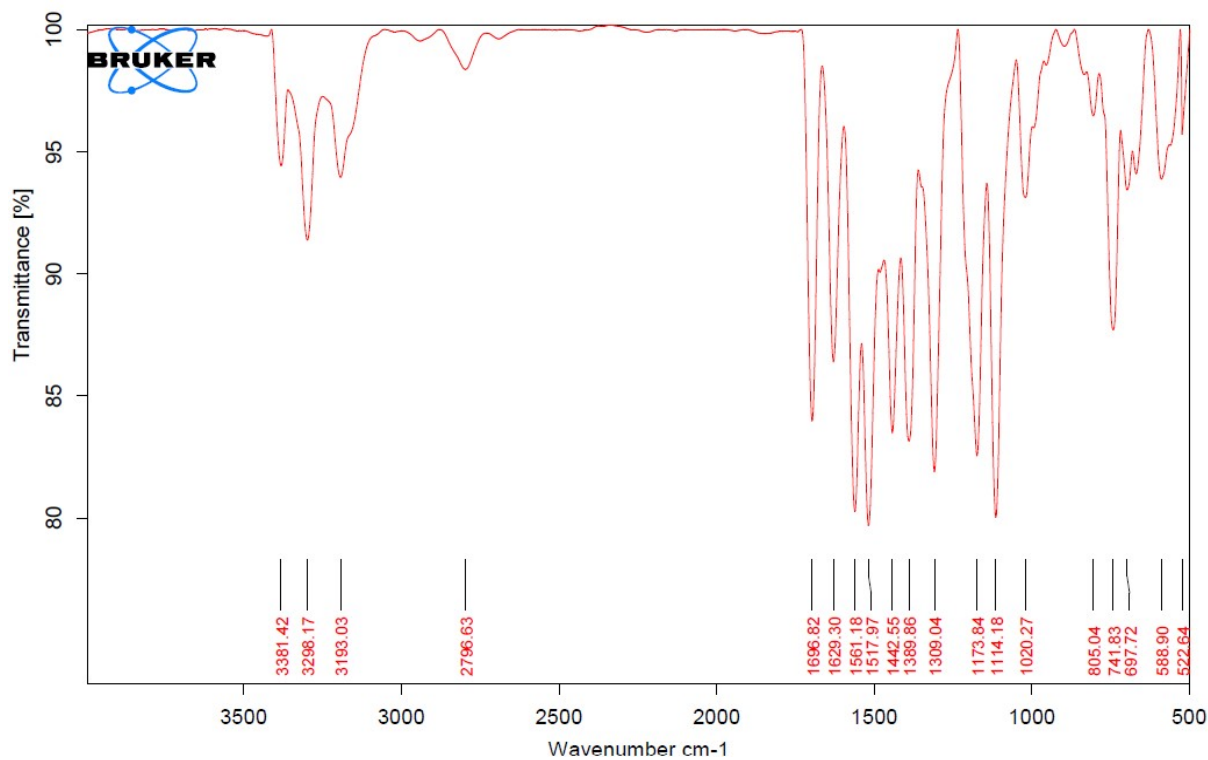
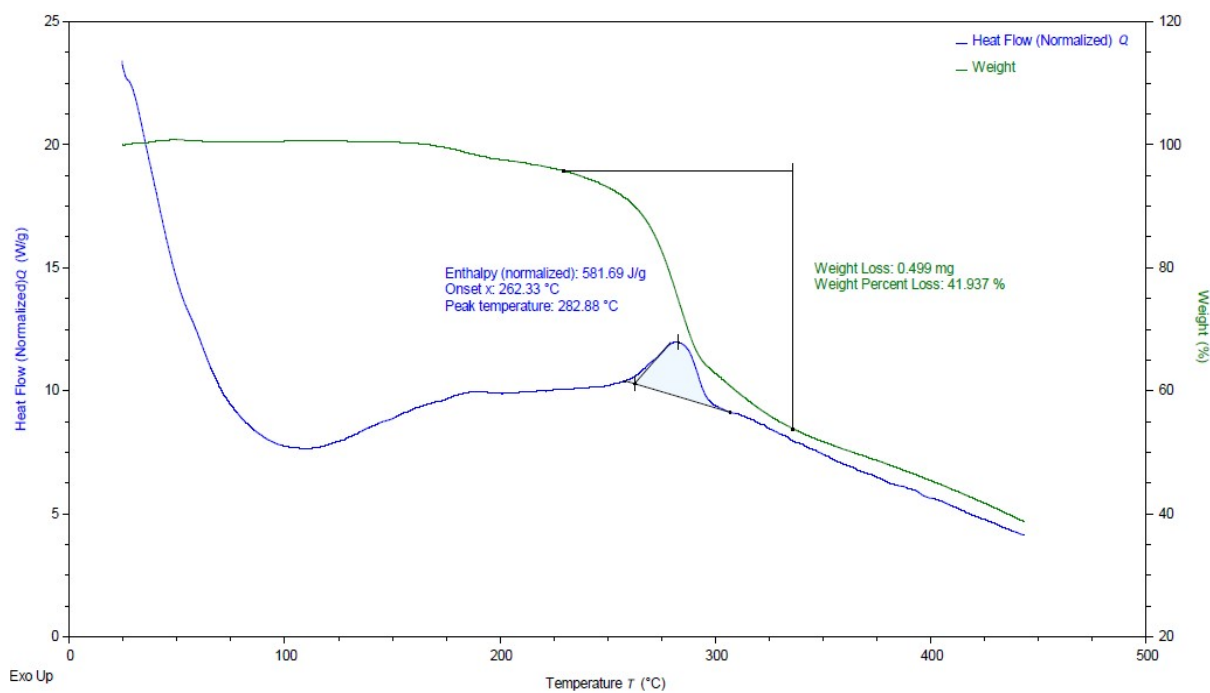


Figure S13: IR spectrum of compound 3.



TA Instruments Trios V5.5.0.323

Figure S14: DSC spectra of compound 3 at heating rate 5 °C min⁻¹.

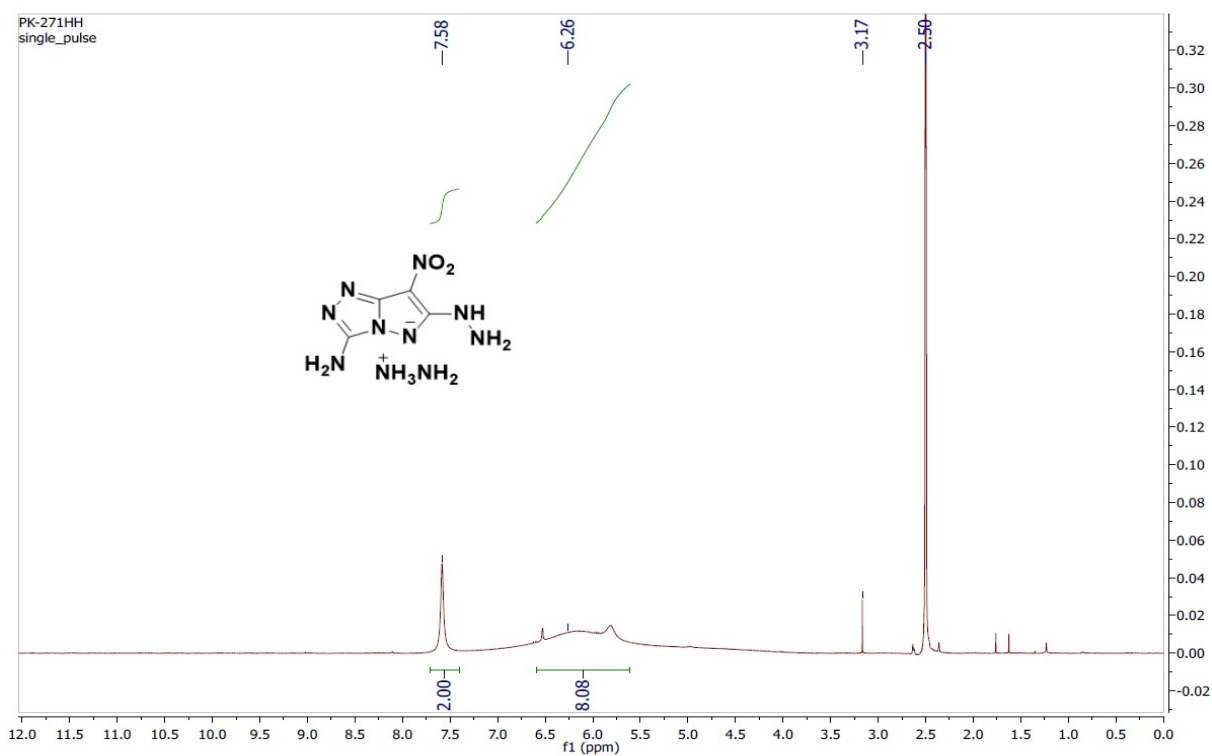


Figure S15: ¹H NMR spectrum of compound 4 in DMSO-*d*₆.

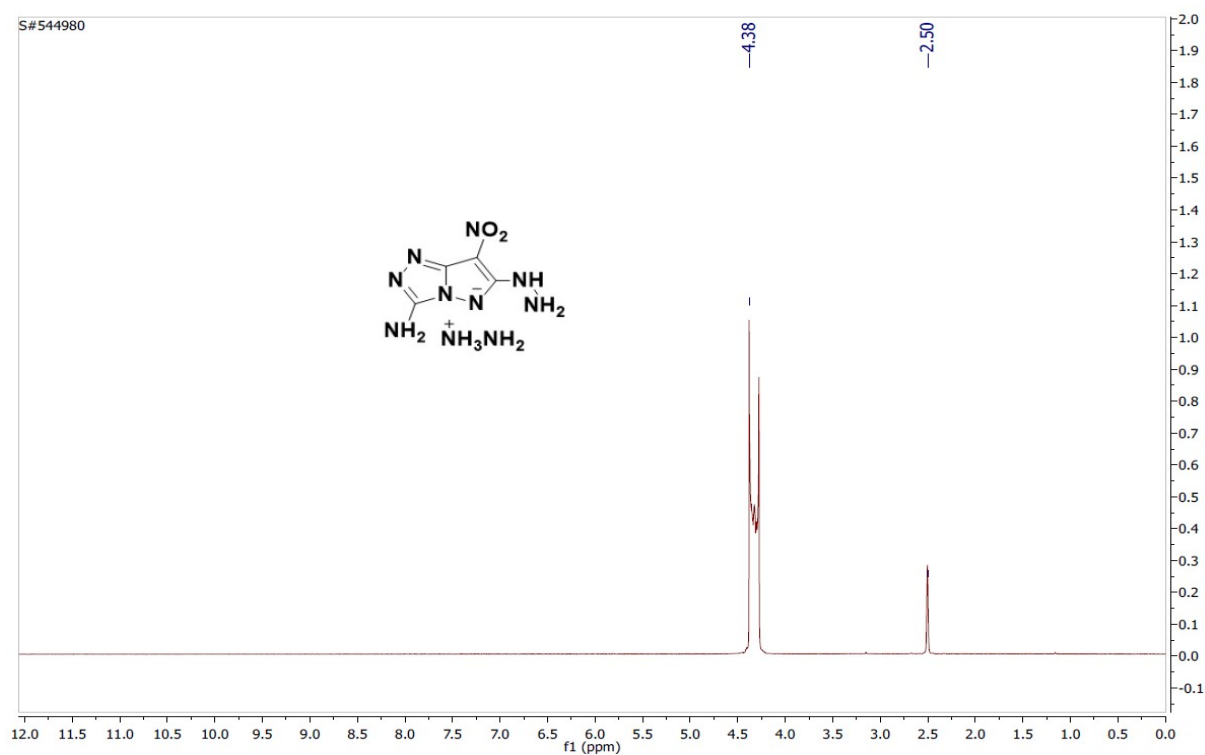


Figure S16: ¹H NMR spectrum of compound 4 in D₂O.

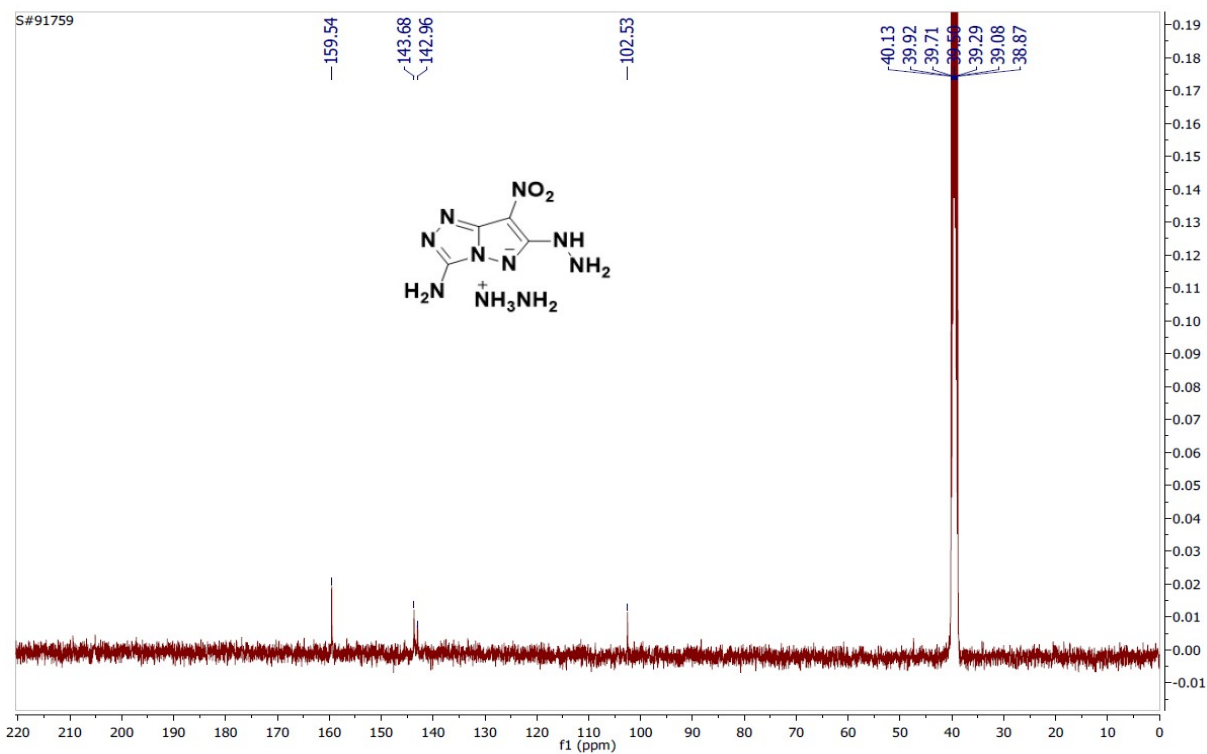


Figure S17: ^{13}C NMR spectrum of compound 4 in $\text{DMSO-}d_6$.

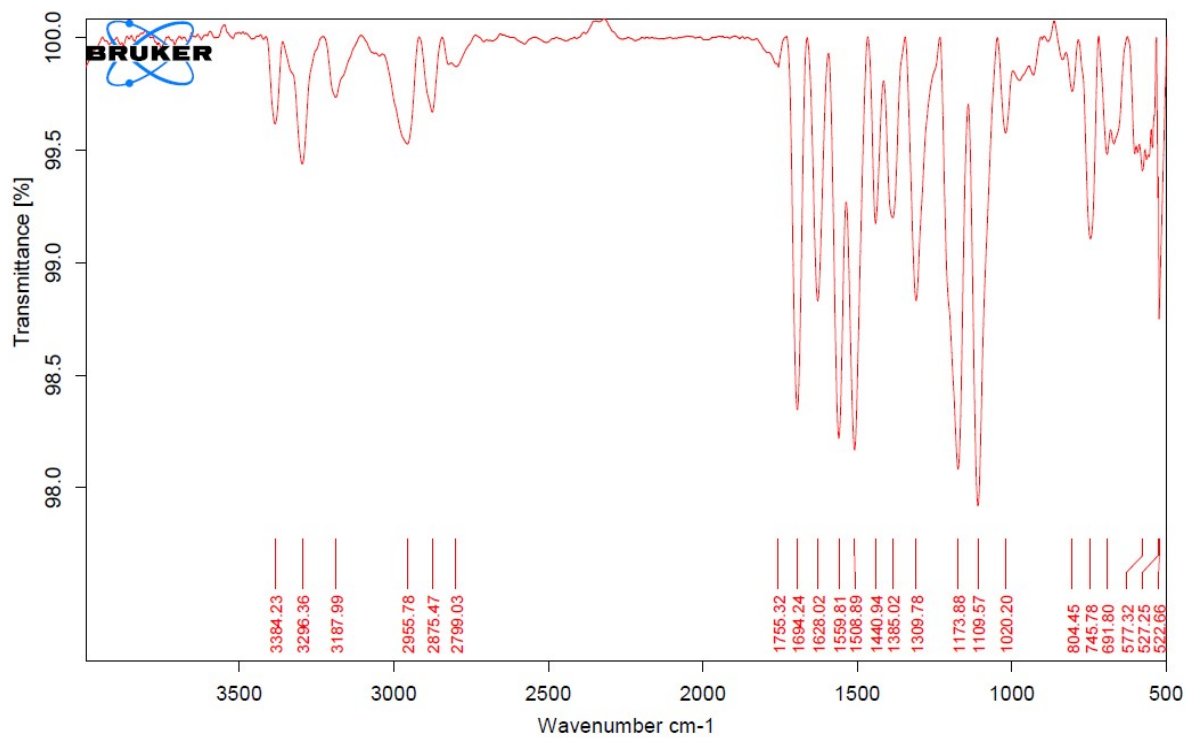
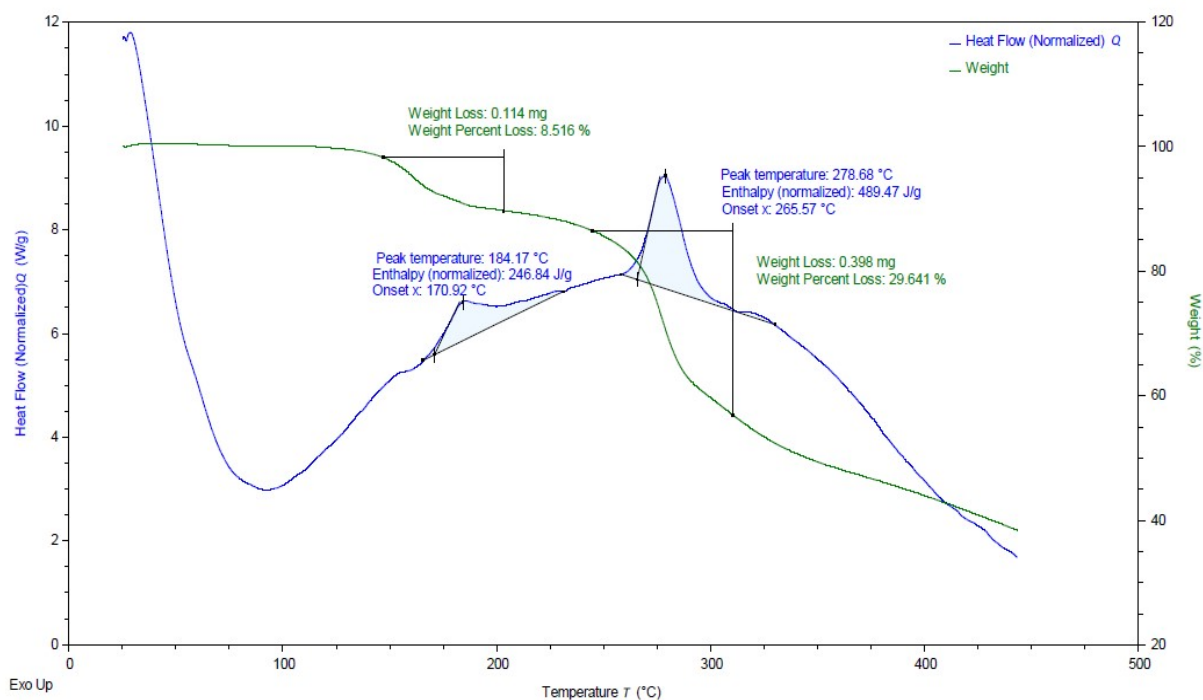


Figure S18: IR spectrum of compound 4.



TA Instruments Trios V5.5.0.323

Figure S19: DSC spectra of compound **4** at heating rate 5 °C min⁻¹.

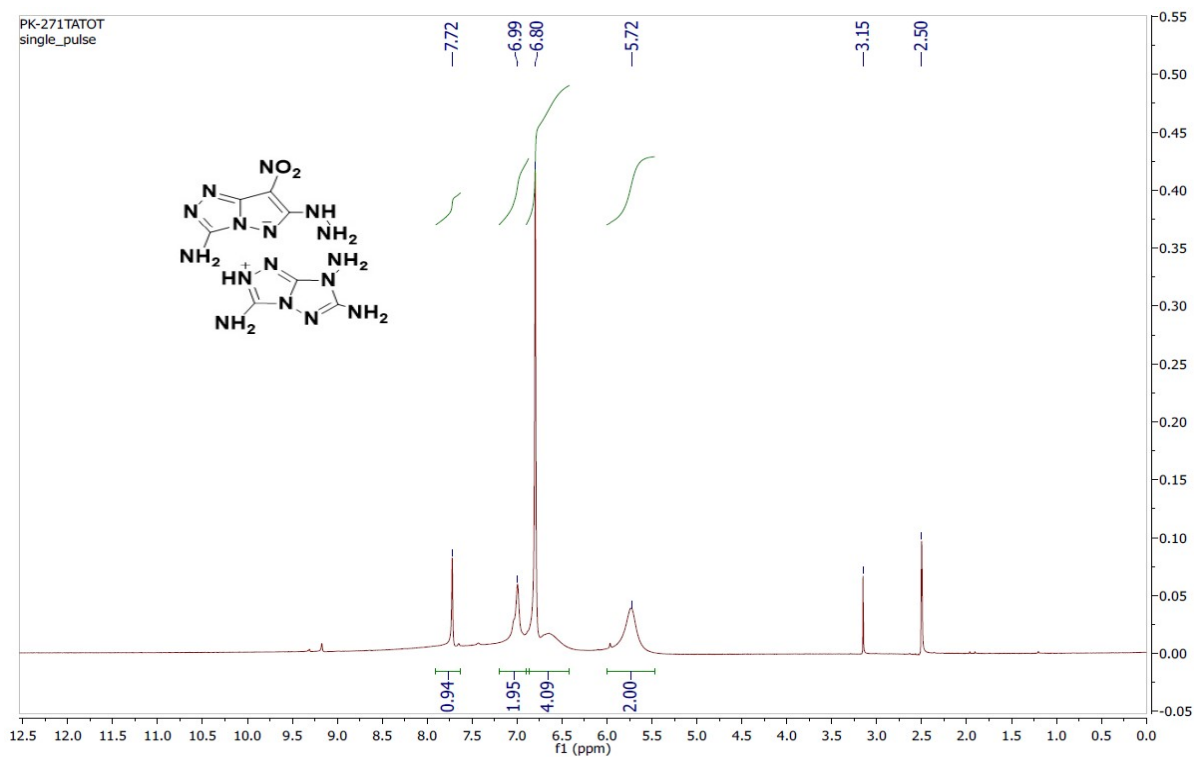


Figure S20: ¹H NMR spectrum of compound **5** in DMSO-*d*₆.

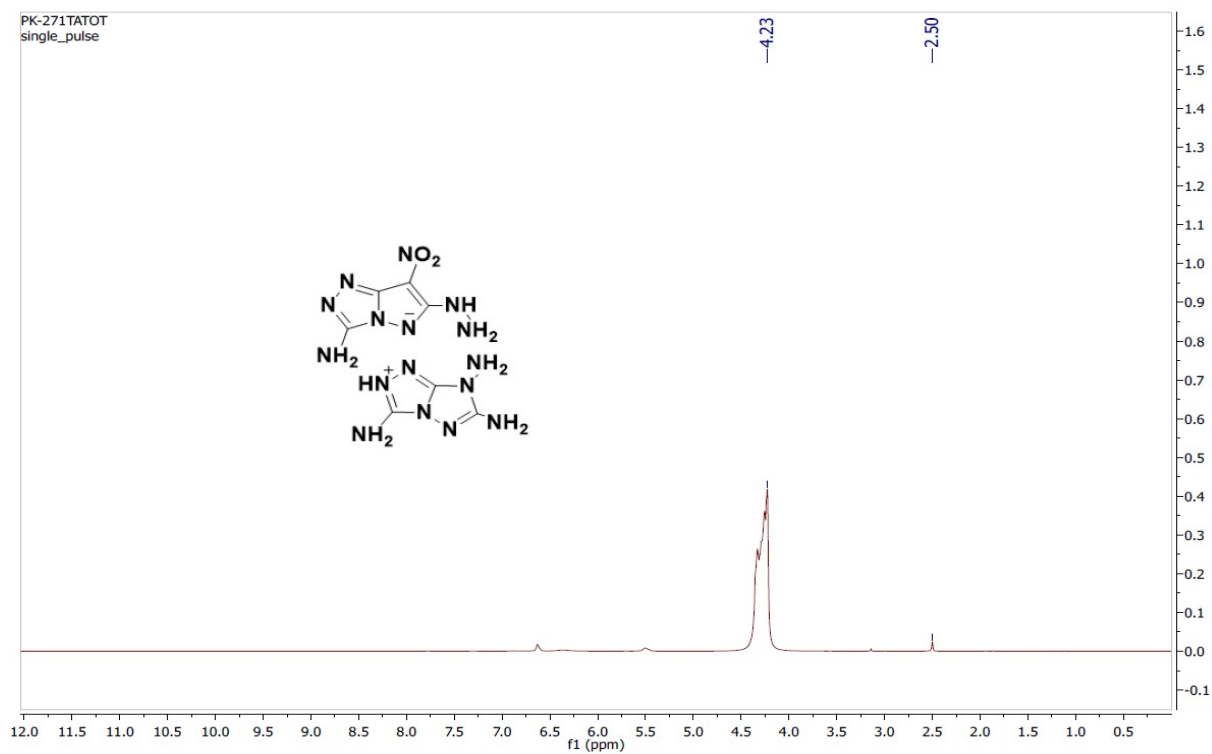


Figure S21: ^1H NMR spectrum of compound **5** in D_2O .

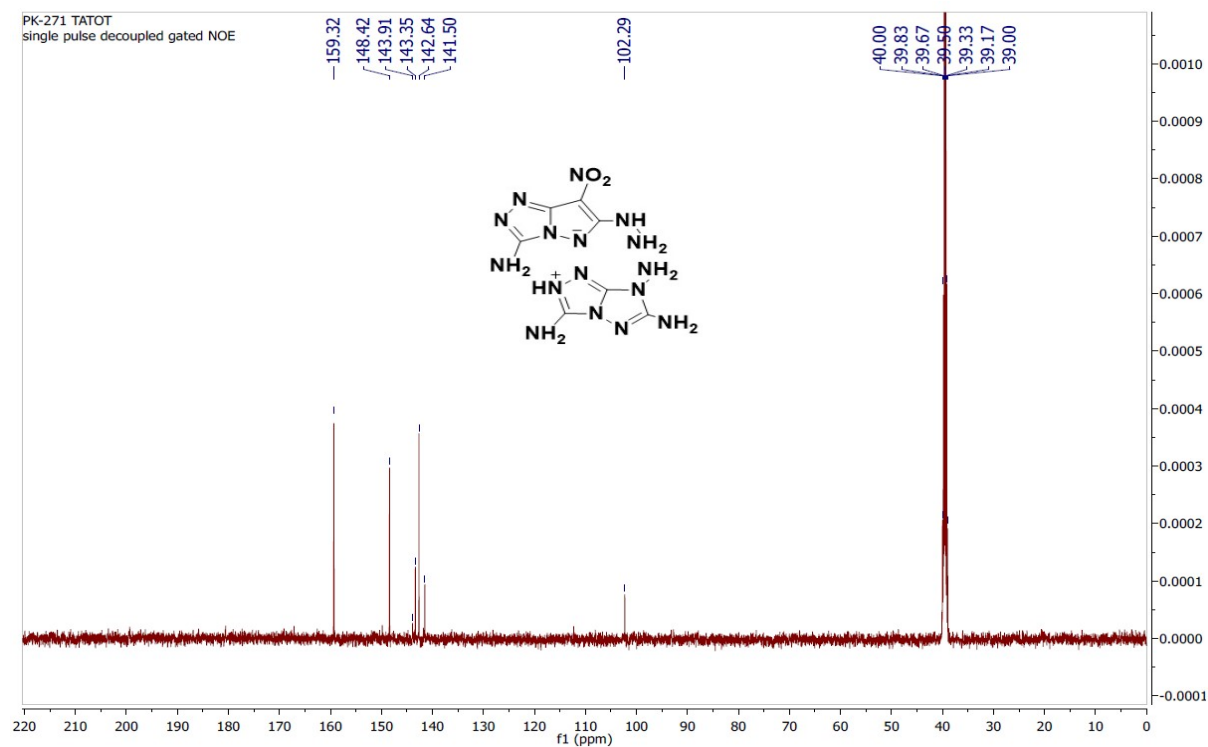


Figure S22: ^{13}C NMR spectrum of compound **5** in $\text{DMSO-}d_6$.

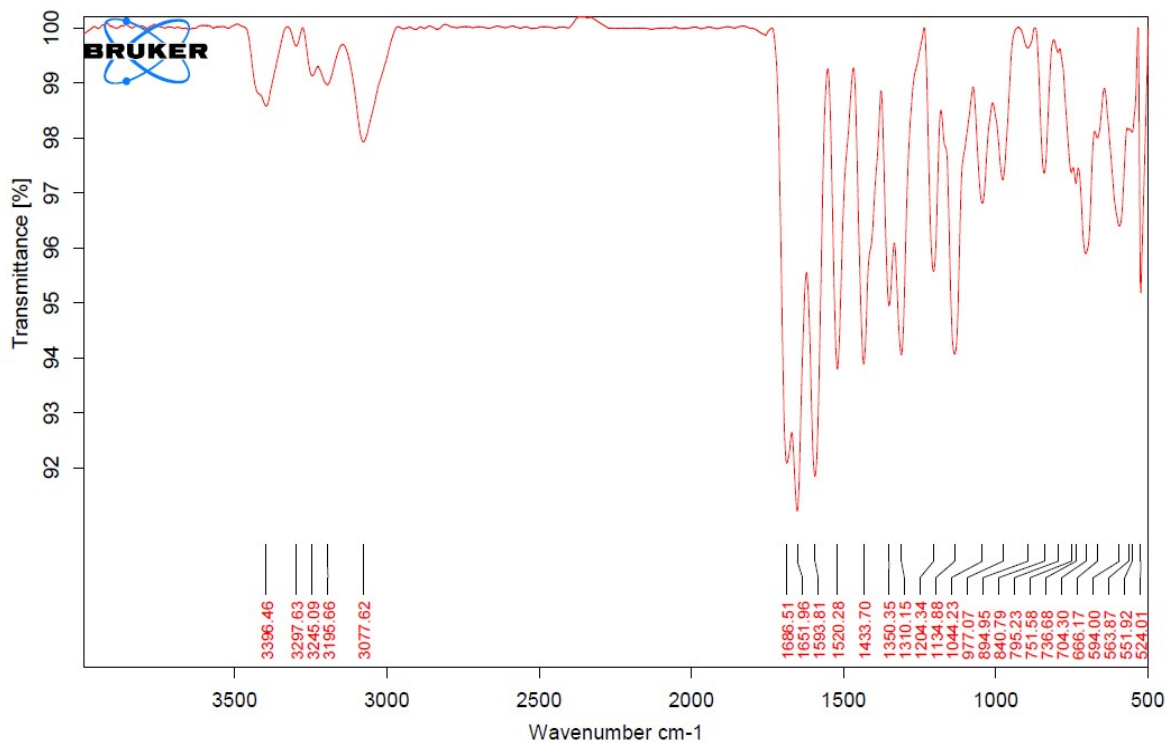
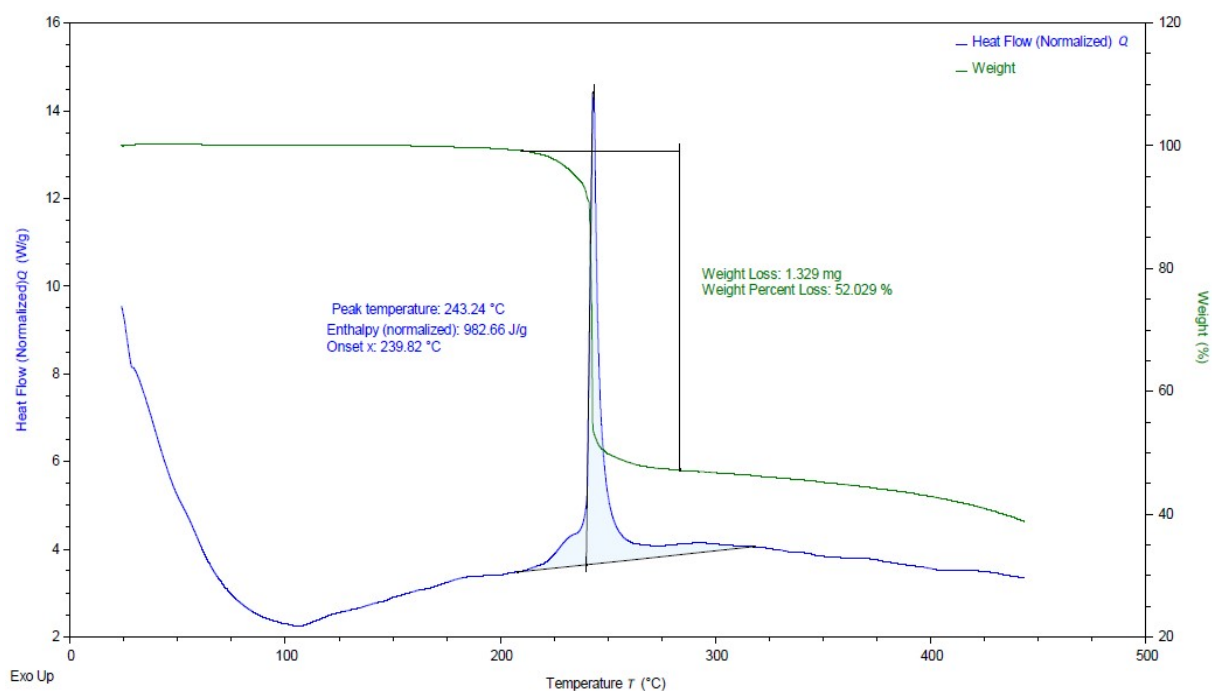


Figure S23: IR spectrum of compound 5.



TA Instruments Trios V5.5.0.323

Figure S24: DSC spectra of compound 5 at heating rate 5 °C min⁻¹.

Computational details

Computations were carried out using the Gaussian 09 program suite.¹ The structure optimizations are performed with M06-2X/def2-TZVPP level of theory and characterized to be true local energy minima on the potential energy surface and no imaginary frequencies were found. Heat of formation (HOF) is a measure of energy content of an energetic material that can decompose, ignite and explode by heat or impact. It enters into the calculation of explosive and propellant properties such as detonation velocity, detonation pressure, heat of detonation and specific impulse. However, it is impractical to determine the HOF of novel energetic materials because of their unstable intermediates and unknown combustion mechanism. The calculated total energies (E_0), zero-point energies (ZPE), and thermal corrections (H_T) at the M06-2X/def2-TZVPP level for the reference compounds used in isodesmic reactions are listed in Table S8. Table S9 lists the total energies (E_0), zero-point energies (ZPE), and thermal corrections (H_T) for target compounds. HOF_{Gas} has been predicted by designing appropriate isodesmic reactions (see Figure S25). In an isodesmic reaction, the number of each kind of formal bond is conserved according to bond separation reaction (BSR) rules. The target molecule is broken down into a set of heavy atom molecules containing same component bonds. BSR rules cannot be applied to the molecules with delocalized bonds and cage skeletons because of large, calculated errors of HOFs. In view of the above, present study involves the design of isodesmic reactions in which the numbers of all kinds of bonds keep invariable to decrease the calculation errors of HOF. Aromatic rings are kept intact while constructing isodesmic reactions.

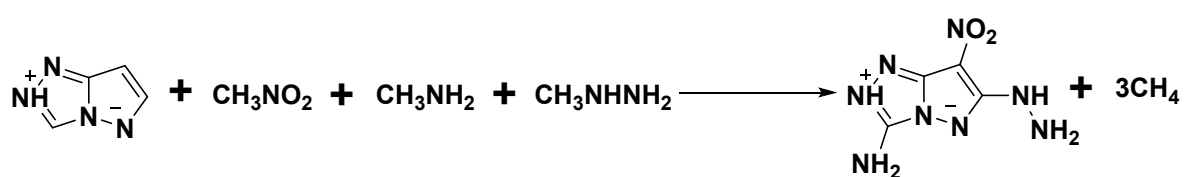


Figure S25. Designed isodesmic reactions for the prediction of gas phase heat of formation (HOF_{Gas}) of target compounds.

The usage of the HOF_{Gas} in the calculation of detonation properties slightly overestimates the values of detonation velocity and detonation pressure, and hence, the solid phase HOF ($\text{HOF}_{\text{Solid}}$) has been calculated which can efficiently reduce the errors. The $\text{HOF}_{\text{Solid}}$ is calculated as the difference between HOF_{Gas} and heat of sublimation (HOF_{Sub}) as,

$$\text{HOF}_{\text{Solid}} = \text{HOF}_{\text{Gas}} - \text{HOF}_{\text{Sub}} \quad (1)$$

The heat of sublimation (HOF_{Sub}), which is required to convert the HOF_{Gas} to the $\text{HOF}_{\text{Solid}}$, was calculated from Equation (2),²

$$\text{HOF}_{\text{Sub}} = 0.000267 A^2 + 1.650087 (v\sigma_{\text{tot}}^2)^{0.5} - 2.966078 \quad (2)$$

Where A represents the surface area of the 0.001 electrons/bohr³ isosurface of electronic density, v denotes the degree of balance between the positive and negative surface potentials, and σ_{tot}^2 is the electrostatic potential variance. These molecular surface properties were obtained using the Multiwfn program³ and listed in Table S10.

Based on the Born–Haber cycle (shown in Figure S26), the heat of formation of an ionic compound can be simplified by subtracting the lattice energy of the salt (H_L) from the total heat of formation of salt (see Table S11) *i.e.* sum of the heats of formation of the cation and anion as shown in equation (3).

$$\text{HOF}(\text{salt}, 298 \text{ K}) = \text{HOF}(\text{cation}, 298 \text{ K}) + \text{HOF}(\text{anion}, 298 \text{ K}) - H_L \quad (3)$$

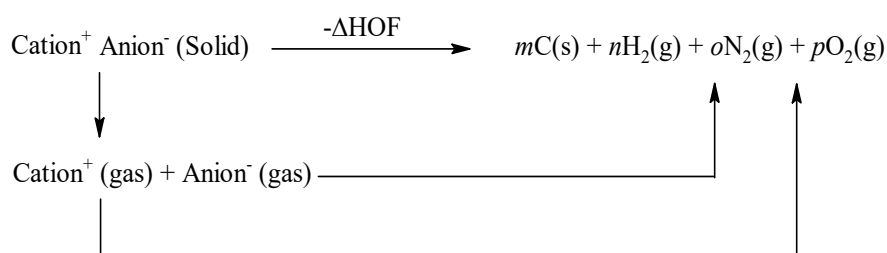


Figure S26. Born-Haber cycle for the formation of energetic salts.

Lattice potential energy is the energy associated with the process in which a crystalline solid lattice, M_pX_q is converted into its constituent gaseous ions, ${}_p\text{M}^{q+}(\text{g})$ and ${}_q\text{X}^{p-}(\text{g})$. The lattice energy can be predicted with reasonable accuracy by using Jenkins' equation (4).⁴

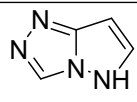
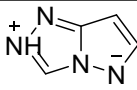
$$H_L = U_{POT} + [p(\frac{n_M}{2} - 2) + q(\frac{n_X}{2} - 2)]RT \quad (4)$$

where n_M and n_X depend on the nature of the ions M_p^+ and X_q^- , respectively, and are equal to 3 for monoatomic ions, 5 for linear polyatomic ions, and 6 for nonlinear polyatomic ions. When lattice potential energy (U_{POT}), is incorporated and made part of a Born–Haber cycle, it needs to be converted into a lattice enthalpy term. This lattice enthalpy (H_L) involves correction of the U_{POT} term by an appropriate number of RT terms. The U_{POT} (kJ mol^{-1}) can be predicted from four different equation (5) as suggested by Jenkins et al.⁴ using following equations,

$$U_{POT} = \gamma(\frac{\rho}{M})^{1/3} + \delta \quad (5)$$

In above equation, ρ is the density (g cm^{-3}).

Table S8. Calculated total energies at 298K (E_0), zero-point energies (ZPE), and thermal corrections (H_T) and experimental HOF_{gas} of reference compounds used isodesmic reaction at the M06-2X/def2-TZVPP level.

Compd.	E_0 (a.u.)	ZPE (au)	H_T (au)	HOF_{gas} (kJ/mol)
CH ₄	-40.453065	0.0449	0.0038	-74.8
CH ₃ NH ₂	-95.776498	0.0644	0.0044	-23.5
CH ₃ NO ₂	-244.955044	0.0506	0.0053	-81
CH ₃ NHNH ₂	-151.077406	0.0824	0.0051	98.65
	-373.651225	0.0882	0.0059	474.36 ^a
	-373.660379	0.0898	0.0060	446.06

^aCalculated using G4 method.

Table S9. Calculated total energies (E_0), zero-point energies (ZPE), and thermal corrections (H_T) for target compounds at the M06-2X/def2-TZVPP level.

Compd.	E_0 (a.u.)	ZPE (au)	H_T (au)	HOF_{gas} (kJ/mol)	$\text{HOF}_{\text{Sublimation}}$ (kJ/mol)
--------	--------------	----------	------------	------------------------------------	--

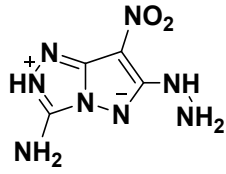
	-744.172489	0.1436	0.0132	500.89	139.15
---	-------------	--------	--------	--------	--------

Table S10. Calculated molecular surface properties of target compounds.

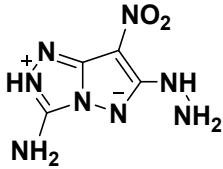
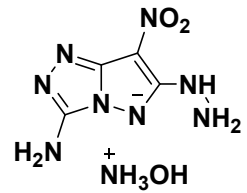
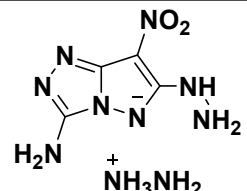
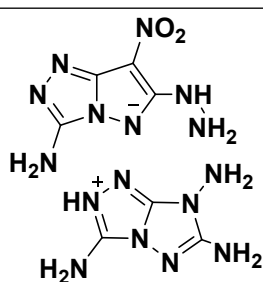
Compd.	Surface area (Å ²)	Volume (Å ³)	σ_{tot}^2 (kcal/mol)	ν
	201.55	200.77	593.53	0.2336

Table S11. Energy content of salts 3-5.

Compd.	HOF _c ^a	HOF _a ^b	U _{Pot} ^c	H _L ^d	HOF _{salt} ^e
	675.6	284.87	495.07	500.02	460.44
	769.5	284.87	494.89	499.84	554.52
	1112.0	284.87	443.13	448.08	948.78

^aHeat of formation of cation (kJ mol⁻¹). HOF_c data for cations is obtained from Ref. 5. ^bHeat of formation of anion (kJ mol⁻¹). ^cLattice potential energy (kJ mol⁻¹). ^dLattice energy (kJ mol⁻¹). ^eHeat of formation of salt (kJ mol⁻¹).

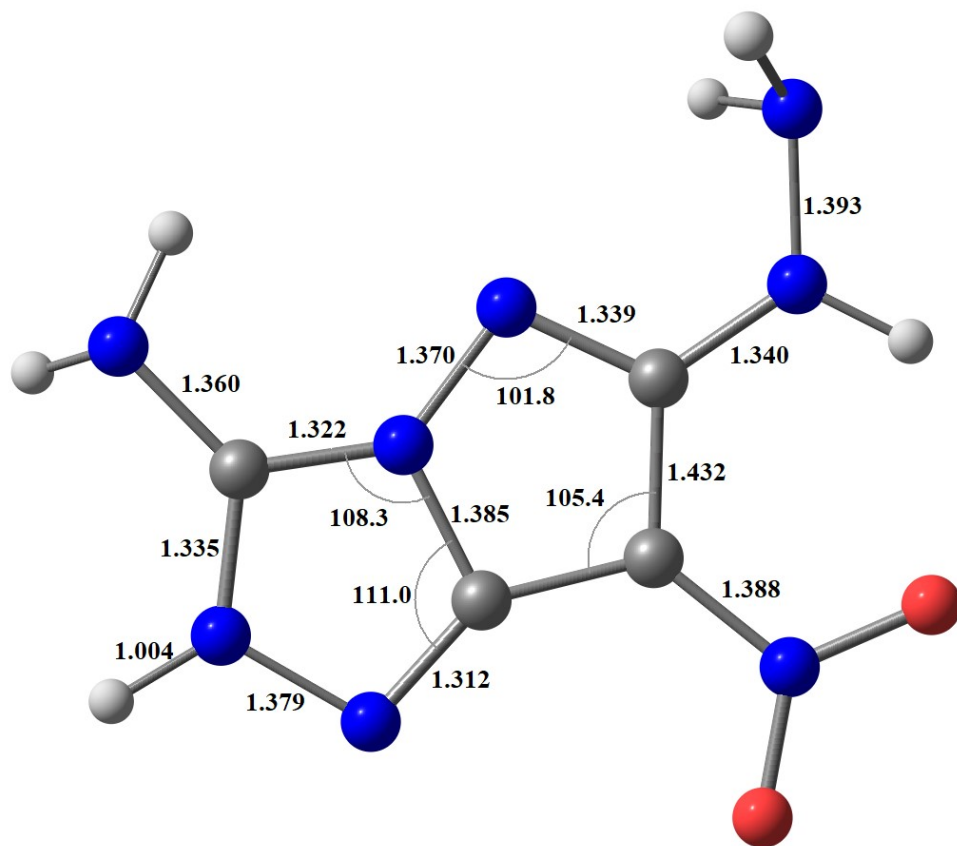


Figure S27. Selective bond lengths (Å) and angles (°) for **2**.

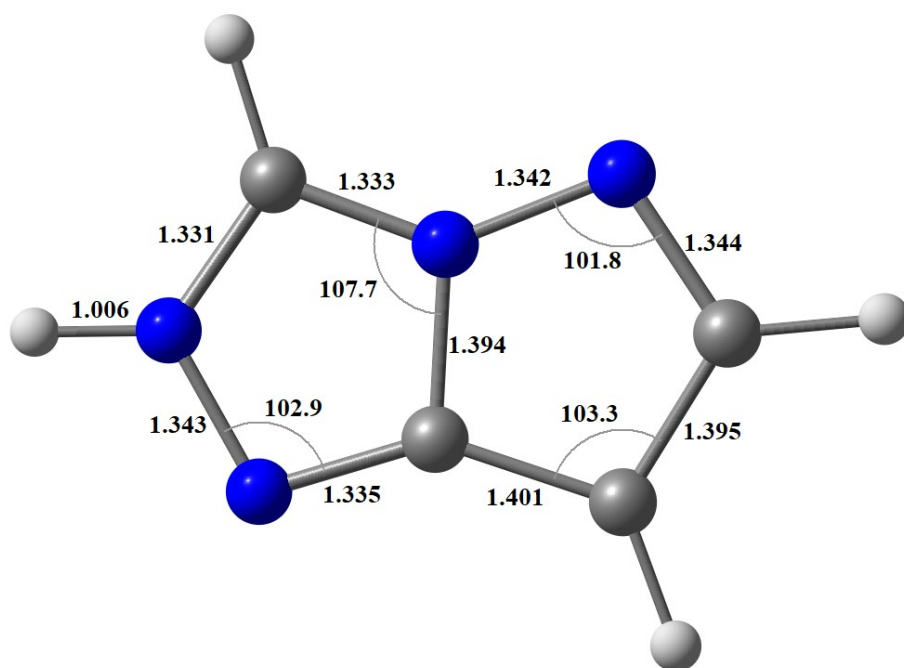


Figure S28. Selective bond lengths (Å) and angles (°) for pyrazolo[5,1-c][1,2,4]triazol-2-ium-5-ide.

Table S12. Optimized coordinates of **2** at M06-2X/def2-TZVPP level of theory.

6	-0.861411000	0.857168000	0.007839000
6	-0.789269000	-0.572865000	0.004394000
6	0.590048000	-0.878273000	-0.004624000
6	2.496155000	0.208537000	-0.003694000
7	1.184374000	0.372727000	-0.008037000
7	1.494674000	-1.828039000	0.004066000
7	2.674563000	-1.114030000	0.000173000
1	3.547146000	-1.609570000	-0.041594000
7	0.338379000	1.450711000	0.001759000
7	3.419949000	1.204015000	-0.068452000
1	3.025261000	2.121126000	0.085059000
1	4.289999000	1.046686000	0.413591000
7	-1.986464000	1.585257000	0.018639000
1	-2.871368000	1.106398000	-0.006575000
7	-1.970535000	2.977363000	-0.013622000
1	-1.471422000	3.315485000	0.802847000
1	-1.440045000	3.278530000	-0.825269000
7	-1.852802000	-1.465057000	0.001114000
8	-1.607677000	-2.657444000	-0.003517000
8	-2.993283000	-0.995892000	0.003389000

Table S13. Optimized coordinates of pyrazolo[5,1-c][1,2,4]triazol-2-ium-5-ide at M06-2X/def2-TZVPP level of theory.

7	-1.959737000	0.062400000	0.000114000
7	-1.237515000	1.194432000	0.000010000
6	-1.242110000	-1.058479000	-0.000065000
6	0.019743000	0.746599000	0.000000000
7	0.026125000	-0.647432000	-0.000046000
6	1.370236000	1.117648000	-0.000094000
6	2.038798000	-0.106646000	0.000177000
7	1.251426000	-1.195309000	-0.000114000
1	-2.963600000	0.122999000	0.000194000
1	-1.612626000	-2.065260000	-0.000124000
1	1.787252000	2.105945000	-0.000174000
1	3.106869000	-0.257055000	0.000247000

Table S14. Optimized coordinates of pyrazolo[5,1-c][1,2,4]triazol-2-ium-5-ide at G4 level of theory.

7	-2.005124000	0.087519000	0.000011000
7	-1.274616000	1.211009000	0.000002000
6	-1.277135000	-1.092553000	0.000001000
6	0.025764000	0.785182000	-0.000011000
7	0.037060000	-0.708969000	-0.000019000
6	1.398653000	1.141555000	-0.000010000
6	2.096770000	-0.102690000	0.000025000
7	1.273183000	-1.208027000	-0.000005000

1	-2.999306000	0.150411000	0.000032000
1	-1.673471000	-2.111107000	-0.000011000
1	1.813717000	2.140422000	-0.000016000
1	3.181224000	-0.239404000	0.000035000

References:

1. Gaussian 09, Revision E.01, M. J. Frisch, G. W. Trucks, H. B. Schlegel, G. E. Scuseria, M. A. Robb, J. R. Cheeseman, G. Scalmani, V. Barone, B. Mennucci, G. A. Petersson, H. Nakatsuji, M. Caricato, X. Li, H. P. Hratchian, A. F. Izmaylov, J. Bloino, G. Zheng, J. L. Sonnenberg, M. Hada, M. Ehara, K. Toyota, R. Fukuda, J. Hasegawa, M. Ishida, T. Nakajima, Y. Honda, O. Kitao, H. Nakai, T. Vreven, Jr. J. A. Montgomery, J. E. Peralta, F. Ogliaro, M. Bearpark, J. J. Heyd, E. Brothers, K. N. Kudin, V. N. Staroverov, R. Kobayashi, J. Normand, K. Raghavachari, A. Rendell, J. C. Burant, S. S. Iyengar, J. Tomasi, M. Cossi, N. Rega, J. M. Millam, M. Klene, J. E. Knox, J. B. Cross, V. Bakken, C. Adamo, J. Jaramillo, R. Gomperts, R. E. Stratmann, O. Yazyev, A. J. Austin, R. Cammi, C. Pomelli, J. W. Ochterski, R. L. Martin, K. Morokuma, V. G. Zakrzewski, G. A. Voth, P. Salvador, J. J. Dannenberg, S. Dapprich, A. D. Daniels, O. Farkas, J. B. Foresman, J. V. Ortiz, J. Cioslowski, D. J. Fox, *Gaussian, Inc.*, Wallingford CT, **2013**.
2. Byrd, E. F. C.; Rice, B. M.; *J. Phys. Chem. A* **2006**, *110*, 1005-1013.
3. Lu, T.; Chen, F.; *J. Comput. Chem.* **2012**, *33*, 580.
4. Jenkins, H. D. B.; Tudela, D.; Glasser, L. Lattice Potential Energy Estimation for Complex Ionic Salts from Density Measurements. *Inorg. Chem.* **2002**, *41*, 2364-2367.
5. Nirwan, A.; Ghule, V. D. Estimation of heats of formation for nitrogen-rich cations using G3, G4, and G4 (MP2) theoretical methods, *Theoretical Chemistry Accounts* **2018**, *137*, 115.